# UNIVERSITY of York

This is a repository copy of *Micromagnetic model of exchange bias : Effects of structure and AF easy axis dispersion for IrMn/CoFe bilayers*.

White Rose Research Online URL for this paper:
http://eprints.whiterose.ac.uk/158379/

Version: Accepted Version

White Rose
university consortium
Universities of Leeds, Sheffield & York

eprints@whiterose.ac.uk
https://eprints.whiterose.ac.uk/

# Micromagnetic model of exchange bias: effects of structure and AF easy axis dispersion for IrMn/CoFe bilayers

**W Daeng-am[1], P Chureemart[1], A Rittidech[1], L J Atkinson[2], R W Chantrell[2], and J Chureemart[1]**

[1]Department of Physics, Faculty of Science, Mahasarakham University, Mahasarakham, 44150, Thailand
[2]Department of Physics, University of York, York YO10 5DD, United Kingdom

E-mail: `jessada.c@msu.ac.th`

**Abstract.** A micromagnetic model of an exchange bias bilayer is used to examine the impact of the physical structure and the easy axis dispersion of the antiferromagnetic (AF) layer on the exchange bias field ($H_{EB}$) in an IrMn/CoFe system. Because of the different timescales, the magnetization dynamics of the IrMn and CoFe layers are modelled using respectively a kinetic Monte Carlo (kMC) approach and Landau-Lifshitz-Gilbert (LLG) equation. The easy axis dispersion is modelled using a Gaussian distribution. The calculations show that $H_{EB}$ increases with increasing IrMn thickness and grain size, in agreement with experimental work. Moreover, the model allows the visualization of the switching process at the micromagnetic level to reveal the reversal mechanism. We find that the effect of AF easy axis distribution not only strongly affects the reduction of $H_{EB}$ but also drives non-coherent behaviour in the reversal mechanism. This confirms that the easy axis distribution is an important factor with strong impact on the magnetic properties and exchange bias field of an exchange bias system.

# 1. Introduction

The interfacial effect currently employed to pin the magnetization direction in devices such as spin valves or Magnetic Tunnel Junctions (MTJ) [1, 2] is the well-known exchange bias (EB) effect [3, 4, 5, 6]. Since the discovery of the phenomenon in 1956 [7] and the first introduction of theoretical description of the exchange bias system in 1957 [8] by Meiklejonh and Bean, numerous experimental and theoretical studies [3, 4, 5, 6] have been carried out in order to understand the physical behaviour behind this effect. Undoubtedly, the effect arises from the interfacial exchange coupling between uncompensated antiferromagnetic (AF) spins and ferromagnetic (FM) spins after field-cooling process [6, 9]. However, studies of several magnetic microstructures demonstrate different characteristics of exchange bias field ($H_{EB}$) because the interface coupling between layers cannot be easily controlled. Therefore, it is important to investigate the role of each magnetic parameter on the properties of the bilayers. Parametric studies of exchange bias investigating the effects of the main parameters accounting for thermal stabilities become increasingly important.

Fulcomer and Charap [10] proposed a model including the distribution of particle size for studying the effect of temperature on exchange bias system and made a comparison with experiment. They found that the consideration of particle size distribution is very significant and is necessary to give agreement between theoretical and experimental results. In 2008, an experimental study of the effect of the particle size distribution in the AF layer in a polycrystalline exchange bias system was reported by Vallejo *et al.* [11, 12]. They found that the exchange bias arises from grains above the critical grain volume $V_C$ (so as to be thermally stable) and below the critical grain volume for setting $V_{SET}$. Using this interpretation, the variation of $H_{EB}$ as a function of grain volume can be predicted, confirming that the grain size distribution is an important factor in exchange bias.

During the deposition process of the exchange bias layers, defects in the polycrystalline films such as grain size distribution and FM/AF interfacial roughness can appear. These effects also cause the misorientation of anisotropy easy axes in both AF and FM layers [13]. Several works have reported that the distribution of anisotropy easy axes is a significant parameter affecting the value of coercivity and the exchange bias field. [14, 15, 16, 17, 18, 19, 20, 21, 22]. The study of magnetically coupled NiFe/NiO layers including the effect of the easy axis distribution was first reported by Zhao *et al.* in ref. [14]. They found that the easy axis misorientation only contributes to the variation of coercivity ($H_c$) with the increasing of NiO thickness due to the appearance of a strong uniaxial anisotropy and no impact on exchange bias field, $H_{EB}$ for relatively thin AF layer. Pogossian *et al.* [20] proposed the model to compare with experimental results by measuring

the easy axis misalignment of FM/AF layers for exchange bias CoFe/NiO system. They reported that $H_{EB}$ and $H_c$ change asymmetrically as a function of FM and AF easy axis dispersion. Moreover, Tarazona *et al.* [21] was also investigated the effect of easy axis distribution of Co/IrMn by varying the film thickness of both materials. They found that the increase of IrMn thickness causes an increase of AF easy axis distribution leading to a reduction of $H_{EB}$ at larger dispersion angle. From the several reports, these show that the effect of AF easy axis misalignment on $H_{EB}$ is still unclear by no change [14], decrease [21], or increase $H_{EB}$ [20, 22] when the film thickness of AF changing. Therefore, it is necessary to study the effect of easy axis dispersion on the variation of $H_{EB}$ in the bilayers system in order to understand its role and physical behind the complex exchange bias phenomena.

There are several models proposed to investigate the exchange bias phenomenon [6, 23, 24], important factors such as the misorientation of easy axis along with the grain size distribution was not taken into account [10]. In the present work, we consequently propose the calculation of $H_{EB}$ in magnetic bilayer systems by using a micromagnetic model which includes the magnetic intra/inter-layer interactions of the FM and AF layers, the effect of grain size distribution, and especially the easy axis misorientation. The details of the model description which combines the different dynamic approaches, kinetic Monte Carlo (kMC) for the AF layer and the stochastic-Landau-Lifshitz-Gilbert (LLG) technique for the FM layer is presented in Sec.II. The model is then used to investigate the crucial parameters of the physical microstructure such as the AF and FM thickness, magnetic grain diameter and also magnetic propeteries such as the AF anisotropy constant and AF easy axis distribution in order to compare with experiment.

# 2. Model description

In order to establish the realistic magnetic bilayer structure, the Voronoi tessellation was employed. Columnar growth is assumed for each grain through the FM and AF layers. The Voronoi construction can control the specified grain size, and grain size distribution with periodic boundary conditions. In addition, the effect of the random easy axis distribution of FM and AF layers are also taken into account using a Gaussian distribution. In this model, both AF and FM grains are assumed to rotate coherently. Fig.1(a) shows the typical structure of bilayers system (top view) with periodic grain boundary at $100 \times 100$ nm$^2$ by Voronoi tessellation. Meanwhile, the typical EB structures whose grains include an easy axis distribution such as perfect alignment of magnetization ($\sigma_\phi = 0°$), the narrow easy axis distribution ($\sigma_\phi = 15°$) and wide easy axis distribution ($\sigma_\phi = 45°$) are illustrated in Fig.1 (b), (c) and (d) respectively.

The FM and AF layers will be modelled with the different techniques in order to describe the different
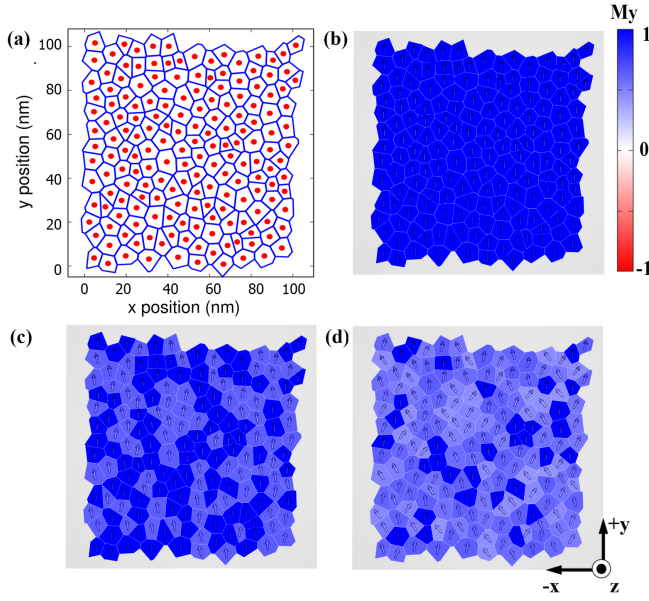
**Figure 1.** Voronoi tessellation of exchange bias system: (a) the typical grain structure with periodic boundary, (b) the perfect alignment of AF anisotropy easy axis orientation ($\sigma_\phi = 0°$), (c) the narrow AF anisotropy easy axis orientation ($\sigma_\phi = 15°$) and the wide AF anistropy easy axis orientation ($\sigma_\phi = 45°$).

magnetic properties, especially the timescale of the magnetization processes. Antiferromangetic material is a high anisotropy material providing the stable exchange bias. Here the timescale varies from seconds to years due to thermally activated magnetization processes. Therefore, the AF layer is treated by a kinetic Monte Carlo (kMC) approach [25] allowing the long-term calculation. Whereas, ferromagnetic material comprising strongly exchange coupled grains reaches equilibrium relatively quickly. Hence, this layer is well described by a standard micromagnetic model with integrating the stochastic-Landau-Lifshitz-Gilbert equation for the dynamics of magnetization in the FM layer.

The magnetization reversal behaviour of the AF layer is simulated using a kMC based model. The magnetization dynamics arises from the thermal activation process described by the Arrhenius-Néel relaxation time. The energy barrier of the system preventing the switching of the grains is described by free energy which depends on the anisotropy constant ($K$), grain volume ($V$) and the total local field acting on each AF grain ($\mathbf{H}_T^{AF}$) shown in detail later. $\mathbf{H}_T^{AF}$ is comprised of the exchange interlayer field acting on the AF grain ($\mathbf{H}_{exch}^{AF}$). To allow calculation of temperature dependent magnetic properties, the magnetic anisotropy constant as a function of temperature will be calculated via using Callen-Callen theory, $K(T) = K(0)[M(T)/M(0)]^n$ from Ref.[26] where $n$ is an exponent which is normally taken as 3.

In this simulation, the origin of exchange bias due to the coupling between AF and FM grains is described in term of the interlayer exchange energy given by Craig *et*

*al.* [27] as the following eq.

$$E_{exch} = -J_s A c \mathbf{m}_{FM} \cdot \mathbf{m}_{AF}, \tag{1}$$

where $J_s$ is the interfacial exchange constant, $A$ is grain area, and $c$ is the contact fraction between grains (here taken as 1). The $\mathbf{m}_{FM}$ and $\mathbf{m}_{AF}$ are the unit vector of FM and AF grains respectively. Subsequently, the $\mathbf{H}_{exch}^{AF}$ acting on AF layer due to the FM layer is given by

$$\mathbf{H}_{exch}^{AF} = \frac{\partial E_{exch}}{\partial \boldsymbol{\mu}_{AF}} = \frac{J_s c \mathbf{m}_{FM}}{M_s t_{AF}} = z H_{ex}^{int} \frac{A}{A_{avg}} \mathbf{m}_{FM}, \tag{2}$$

where $\boldsymbol{\mu}_{AF} = M_s V_{AF}, \mathbf{m}_{AF}$ is the moment of AF grain. $M_s$ is the saturation magnetization, $V_{AF} = A t_{AF}$ is AF grain volume. $z = t_{FM}/t_{AF}$ is the fraction of film thickness, $t_{FM}$ is the FM thickness, $t_{AF}$ is the AF thickness, and $A_{avg}$ is the average value of all grain areas in the system. $H_{ex}^{int}$, representing the intrinsic exchange field acting on AF layer due to FM layer, is

$$H_{ex}^{int} = \frac{J_s c}{M_s t_{AF}}. \tag{3}$$

In order to calculate the energy barrier of AF layer, the following form of the Stoner-Wohlfarth energy is used for the AF grains:

$$E = -K_{AF} V_{AF} (\mathbf{e} \cdot \mathbf{m}_{AF})^2 - J_s A c \mathbf{m}_{FM} \cdot \mathbf{m}_{AF}, \tag{4}$$

where $K_{AF}$ is AF anisotropy constant and $\mathbf{e}$ is the easy direction of AF magnetization. The first and second terms of Eq.(4) represent the anisotropy energy and the total field energy which is comprised of the interlayer exchange energy acting on AF layer respectively. Hence, the randomly AF easy axis distribution is then taken into account for the calculation of AF/FM coupling. The magnetization dynamics is driven by thermal activation processes over the energy barriers on a timescale given by the Arrhenius-Néel law:

$$\tau^{-1} = f_0 \exp(-KV/k_B T). \tag{5}$$

The minimum energy required for preventing superparamagnetic state with a measurement time of 100 s and typical value of attempt frequency $f_0 \approx 10^9$ s$^{-1}$ is $25 k_B T$. The total relaxation time used to calculate the transition probability in Eq.(6) is $\tau^{-1} = \tau_{12}^{-1} + \tau_{21}^{-1}$. The transition probability of each grain [25, 28] is given by

$$P_t = (1 - e^{-t_m/\tau}), \tag{6}$$

where $t_m$ is the measuring time and $\tau$ is the Arrhenius-Neel relaxation time calculated via Eq. 5. The total energy barrier including the effect of easy axis misorientation is written, using the Pfeiffer approximation [29] as

$$E_b(\mathbf{H}_T^{AF}, \theta_H) = KV[1 - \mathbf{H}_T^{AF}/g(\theta_H)]^{\kappa(\theta_H)}, \tag{7}$$

where $g(\theta_H) = [\cos^{2/3}\theta_H + \sin^{2/3}\theta_H]^{-3/2}$ and $\kappa(\theta_H) = 0.86 + 1.14g(\theta_H)$. magnetization switching of a grain is allowed with a probability given by Eq. 6.

Meanwhile, in the FM layer the standard micromagnetic model is used to describe the magnetization dynamics based on the stochastic-Landau-Lifshitz-Gilbert (LLG) equation as

$$\frac{\partial \mathbf{M}}{\partial t} = -\frac{\gamma}{(1+\alpha^2)}\left\{(\mathbf{M}\times\mathbf{H}_{eff}) + \alpha[\mathbf{M}\times(\mathbf{M}\times\mathbf{H}_{eff})]\right\},$$
(8)

where $\mathbf{M}$ is the magnetization, $\alpha$ is the Gilbert damping constant, $\gamma$ is the gyromagnetic ratio, and $\mathbf{H}_{eff}$ is the net effective field acting on each grain given as

$$\mathbf{H}_{eff} = \mathbf{H}_{anis} + \mathbf{H}_{exch} + \mathbf{H}_{dip} + \mathbf{H}_{app} + \mathbf{H}_{th} + \mathbf{H}_{exch}^{FM},$$
(9)

which includes the anisotropy field ($\mathbf{H}_{anis}$), the exchange field ($\mathbf{H}_{exch}$) between nearest neighbour grains, the dipolar field ($\mathbf{H}_{dip}$), the external field ($\mathbf{H}_{app}$) applied in-plane, the thermal field ($\mathbf{H}_{th}$) as well as the exchange interlayer field ($\mathbf{H}_{exch}^{FM}$) between FM/AF layers due to the exchange bias effect.

Within the FM layer, the intergranular exchange field strength $H_{ex}$ is given by Peng *et al.* [30] as follows:

$$\mathbf{H}_{exch}^{ij} = H_{ex}\left(\frac{J_{ij}}{J_m}\right)\left(\frac{L_{ij}}{L_m}\right)\left(\frac{A_m}{A_i}\right)\mathbf{m}_j,$$
(10)

where $H_{ex} = J_m L_m/(a^2 M_s A_m)$ and $\mathbf{m}_j$ represents the unit vector of grain $j$. Finally, the exchange field acting on an FM grain from the AF layer is

$$\mathbf{H}_{exch}^{FM} = H_{ex}^{int}\frac{A_i}{A_{avg}}\mathbf{m}_{AF}.$$
(11)

It is noted that this micromagnetic model of exchange bias starts with the process after the field cooling which is the FM layer coupled with AF layer by the exchange interlayer field.

## 3. Results

In this work, the magnetic bilayer system is investigated using typical magnetic parameters of the current FM and AF materials for read sensors, specifically CoFe and IrMn respectively. The computational cell is set as lateral system size of $100 \times 100$ nm$^2$ and the median grain diameter at 8 nm. Periodic boundary conditions were used. The grain size distribution is lognormal with a standard deviation of $\sigma_{lnD} = 0.2$ [31]. The magnetic parameters of CoFe and IrMn layers used in this calculation are as follows: Curie temperature, $T_c$ = 1300 K, saturation magnetization, $M_s$ = 1800 emu/cc, and $K_{FM}$ = $1.8 \times 10^5$ erg/cc. For the IrMn layer, the Néel temperature and anisotropy constant are set as $T_N$ = 690 K and $K_{AF} = 3 \times 10^6$ erg/cc [27, 32] respectively. The exchange interlayer field strength ($H_{ex}^{int}$) is an unknown parameter which relates with the interface exchange coupling between FM and AF layers [27]. In

this work, $H_{ex}^{int}$ is selected at a value of 250 Oe and 500 Oe which gives reasonable value of exchange bias field for IrMn/CoFe in experimental work [33] for initial calculation. Then, $H_{ex}^{int}$ representing the exchange coupling between FM and AF layers is set to 250 Oe for all calculations.

In order to fully understand the exchange bias phenomenon in read head sensor including the random easy axis and grain size distribution for realistic model, we used the micromagnetic model to investigate the thermal stability and the effects of the physical structure such as the effects of the film thickness of FM and AF layers and the magnetic grain diameter. Particularly, we consider the impact of the random easy axis distribution in the AF layer. The bilayer system is set with lateral system size of $100 \times 100$ nm$^2$ at a finite temperature 300 K. We start by considering a system with perfect alignment of AF easy axes, which gives agreement with the experimental results of Vallejo-Fernandez *et al.*[11]. Subsequently, this model will be used to investigate the effects of the random easy axis distribution and the grain distribution leading to different behaviour of exchange bias field. In general the easy axis angular dispersion is Gaussian with a standad deviation $\sigma_\phi$).
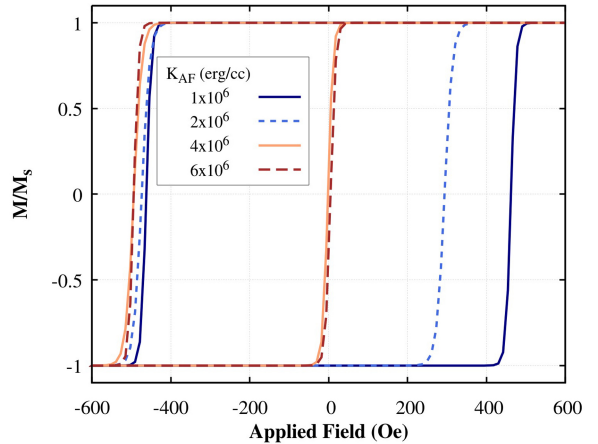


**Figure 2.** Hysteresis loops of IrMn/CoFe bilayer system as a function of AF anisotropy constant at 300 K.

### 3.1. Perfect alignment case

The most important factor for exchange bias phenomenon in the FM/AF bilayer structure is the anisotropy constant of AF layer $K_{AF}$, which provides thermal stability of EB devices. Consequently, we first calculate the effect of $K_{AF}$ on the hysteresis loop and exchange bias field $H_{EB}$, defined by $H_{EB} = (H_- - H_+)/2$ [5], as shown in Fig.2. It is seen that for small $K_{AF}$ of $1 \times 10^6$ erg/cc, the hysteresis loop is barely shifted. However, the loop coercivity, defined by $H_c = (H_- + H_+)/2$, increases. This is due to switching of the AF layer as the exchange field from the FM layer switches. As a result the exchang bias from the AF layer opposes switching in both directions leading to a symmetric loop with enhanced coercivity. On increasing the value of $K_{AF}$, the loop coercivity decreases and shifted

loops appear indicating the onset of exchange bias. The increasing AF anisotropy resists switching and gives rise to a unidirectional energy contribution which provides the exchange bias. Moreover, the hysteresis loops shown in Fig.2 are almost completely square. It is noted that the squareness of the loop reflects the fact that we include no pining sites in the model.
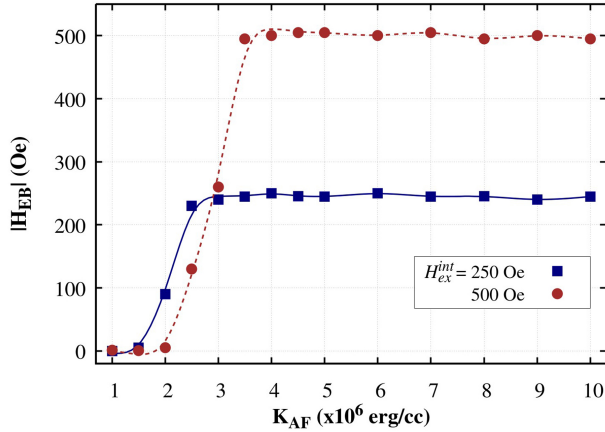


**Figure 3.** The variation of $H_{EB}$ with AF anisotropy constant for different values of $H_{ex}^{int}$ = 250 and 500 Oe. The lines are used to guide for the eyes.

In order to further investigate the behaviour of the exchange bias phenomenon, we extract the value of $H_{EB}$ as a function of $K_{AF}$ from the hysteresis loops as mentioned above. The results are presented in presented in Fig.3. In this case, the variation of $H_{EB}$ with two different $H_{ex}^{int}$ values of 250 Oe and 500 Oe is compared. The result shows that in each case the magnitude of $H_{EB}$ increases with increasing $K_{AF}$ leading asymptotically to a maximum value. The onset of $H_{EB}$ is at $1.5 \times 10^6$ erg/cc and $2 \times 10^6$ erg/cc for $H_{ex}^{int}$, 250 Oe and 500 Oe respectively. In the following $K_{AF}$ around $3 \times 10^6$ erg/cc is used for our calculations which is consistent with the measurement of $K_{AF}$ in IrMn/CoFe bilayer system [32].

It is well known that the exchange bias phenomenon is involved with the effects of physical microstructure such as grain diameter and film thickness dependence of both FM and AF layers relating to energy barrier. In order to establish the intrinsic effect of the microstructure on the thermal stability, we firstly consider the exchange bias field, $H_{EB}$ with the perfect alignment case of easy axis orientation, $\sigma_\phi = 0°$. The simulations have been done via two separate procedures, studying first the film thickness dependence of the EB properties and secondly the grain diameter dependence. The lateral system size and the details of the magnetic properties of CoFe and IrMn layers are given in Sec.2. The thickness dependence effect on $H_{EB}$ is first investigated by considering systems with constant IrMn thickness CoFe(t)/IrMn(4nm) and and constant CoFe thickness CoFe(4nm)/IrMn(t), where t is varied from 2 to 10 nm at fixed grain diameter of 8

nm. Fig.4 shows the variation of $H_{EB}$ with the film thickness of the FM and AF layers. It is clear that $H_{EB}$ increases rapidly with the increasing of AF thickness, reaching a maximum at 5 nm and beyond. Below 2 nm thickness the AF layer presents thermal instability due to the superparamagnetic behaviour [10, 6] and the exchange bias vanishes. On the other hand, increasing the FM thickness leads to a decrease in $H_{EB}$. At large thickness $H_{EB}$ is approximately $\propto 1/M_{FM}t_{FM}$ in accordance with simple theoretical expectations [34]. However, a plateau is reached for low thickness. predicted results give the same trend as the previous experiments [12, 35]. Specifically, we could compare the AF and FM thickness dependence of $H_{EB}$ predicted by our model with the experimental investigations in Ref. [12] and Ref. [35] respectively as shown in Fig.4 (inset). Vallejo-Fernandez *et al.* carried out the measurement of $H_{EB}$ in the samples Si/Cu(10 nm)/CoFe(2.5 nm)/IrMn ($t_{AF}$)/Ta(10 nm) with different AF thicknesses ranging from 3 to 12 nm. The measurements were performed at room temperature. The results showed that $H_{EB}$ increases sharply with increasing $t_{AF}$ to the maximum point at around $t_{AF}$ = 8 nm and decreases slightly for the thick AF layer. Meanwhile, Lee *et al.* also showed the variation of exchange field which was inversely proportional to the thickness of ferromagnetic layer in the samples Ta/AlO$_x$/CoFe($t_{FM}$)/IrMn(10nm)/NiFe/Ta with different FM thicknesses ranging from 3.5 nm to 8.75 nm as shown in Fig.4 (inset). This confirms that the trends of the predicted results give good agreement with the experiments as shown in Fig.4 [12, 35].
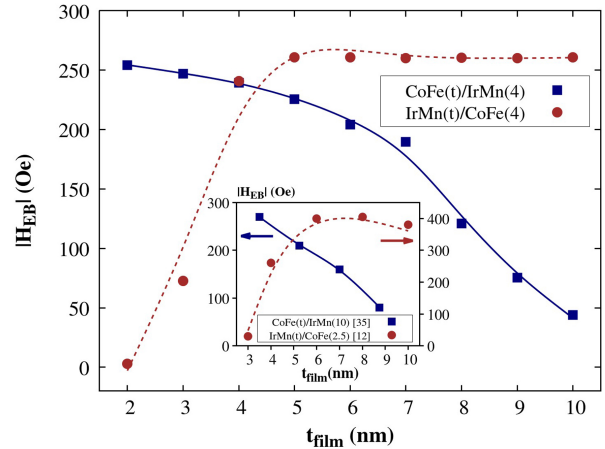


**Figure 4.** The variation of $H_{EB}$ with film thickness dependence at fixed grain diameter of 8 nm comparing with experiment as an inset. Data taken from [12, 35]. The square symbols show the CoFe thickness dependence and the circle symbols show the IrMn thickness dependence (The lines are used to guide for the eye).

The effect of grain volume dependence on $H_{EB}$ is next investigated as shown in Fig.5. In order to observe the effect of AF grain volume which is crucial factor for thermal stability, the grain diameter is varied from 4 to 10 nm with three different IrMn thicknesses ($t_{IrMn}$ = 4, 6

and 8 nm) whereas the thickness of FM layer is fixed at 4 nm. It is noted that our calculations with grain diameter dependence can be compared with experimental work [6] using films prepared by a HiTUS sputtering system. We found that our simulation results show similar trends of the variation of $H_{EB}$ as a function of grain diameter at different AF thickness with experimental results as shown in Fig.5 (inset). At small diameter and thin AF thickness, the exchange bias is thermally unstable with no loop shift while the exchange bias field increases with increasing diameter and film thickness of AF layer. The trend of the variation of $H_{EB}$ as a function of grain diameter for the different $t_{IrMn}$ shows similar behaviour. This is due to the fact that the increases diameter and thickness increase the energy barrier and also increase the fraction of thermally stable AF state which are proportional to the AF grain volume shown by O'Grady *et al.* in Ref.[6].
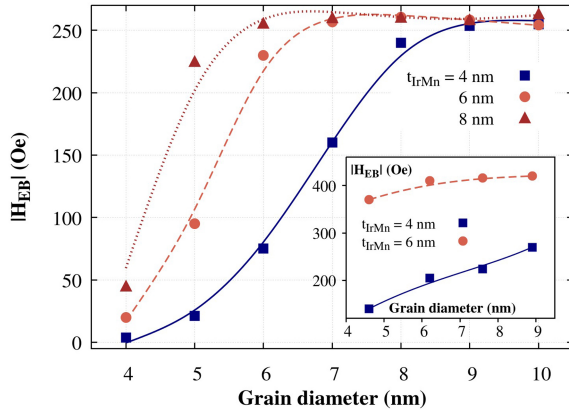


**Figure 5.** The grain diameter dependence on $H_{EB}$ for three different cases of IrMn thickness = 4, 6 and 8 nm comparing with experiment as an inset. Data from [12] (connected by lines as a guide for the eye).

### 3.2. The effect of easy axis distributions

During the experimental procedures of synthesis for providing the exchange bias layers, the magnetic field must be applied into the system in order to induce the easy axis direction of FM layer and also aligns the an easy axis in AF layer along the applied field at the interface. This process can lead to establishment of some degree of AF easy axis distribution due to the heating process and the thermal stability of large AF grains (stable) [10, 18, 36]. Moreover, defects in the polycrystalline films such as grain size distribution and interfacial roughness during the growth process can occur. These effects also enhance the misalignment of anisotropy easy axes in AF layer. Several experimental works have reported the influence of the AF easy axis dispersion which causes an increase [20, 22] or decrease [21] of $H_{EB}$. These show that the effect of AF easy axis misalignment on $H_{EB}$ is still unclear. Therefore, we applied our micromagnetic model of the exchange bias to investigate the AF easy axis dispersion

effect on the variation of $H_{EB}$ values. The visualization of the magnetization dynamics of AF/FM interfacial layer from calculation is also displayed in order to reveal the reversal mechanism and understand the physics behind the mechanism of the reversal process and the effects of the AF anisotropy easy axis distribution.
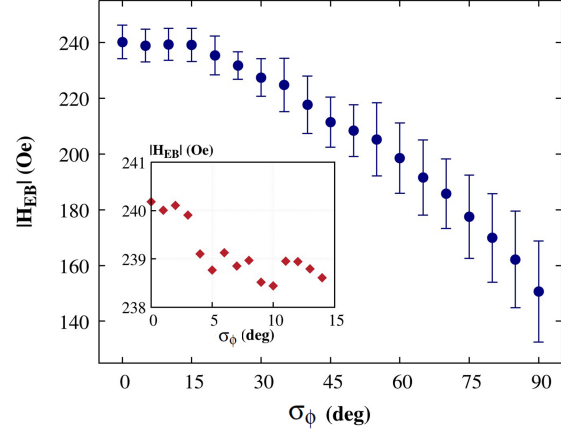


**Figure 6.** The change of $H_{EB}$ as a function of dispersion angle $\sigma_\phi$ varied from $0°$ upto $90°$. The inset shows exchange bias field for small dispersion angle.

The existence of AF anisotropy easy axis distribution arises from the underlying physical mechanism in exchange bias systems. In order to demonstrate the role of AF anisotropy easy axis distribution in exchange bias system, the variation of exchange bias field is investigated by varying the dispersions of AF easy axis orientation from $0°$ to $90°$ with steps of $5°$. Microstructures were generated to give a log-normal distribution, LND of $\sigma_{LND} = 0.2$. 50 statistically different structures were simulated and the mean and standard error are calculated. In this case, the exchange bilayer system is set with lateral system size of $100 \times 100$ nm$^2$, the thickness of CoFe(4nm)/IrMn(4nm), diameter at 8 nm, $K_{FM} = 1.8 \times 10^5$ erg/cc, $K_{AF} = 3 \times 10^6$ erg/cc and $H_{ex}^{int} = 250$ Oe.

Fig.6 shows the variation of the average value of $H_{EB}$ as a function of AF easy axis distribution, $\sigma_\phi$. The result shows that, for small values of the AF easy axis dispersion, $H_{EB}$ is reasonable constant, although the inset in Fig.6 shows a slow decrease. This indicates that the reduction in $H_{EB}$ is not due to switching of the AF grain spin directions, since for coherent rotation the decrease of switching field with angle is most pronounced for small angles. For $\sigma_\phi > 15°$ there is a pronounced decrease in $H_{EB}$, likely due to the reduction of the exchange field acting on the FM due to the orientation of the AF grain spin directions away from the pinning direction.

We now proceed to reveal the AF easy axis dispersion effect on the reduction of $H_{EB}$ by observation of the magnetization reversal mechanism at the different applied field values, specifically the positive saturation field, zero applied field, $\mathbf{H}_{app}$ = -450 Oe and the negative
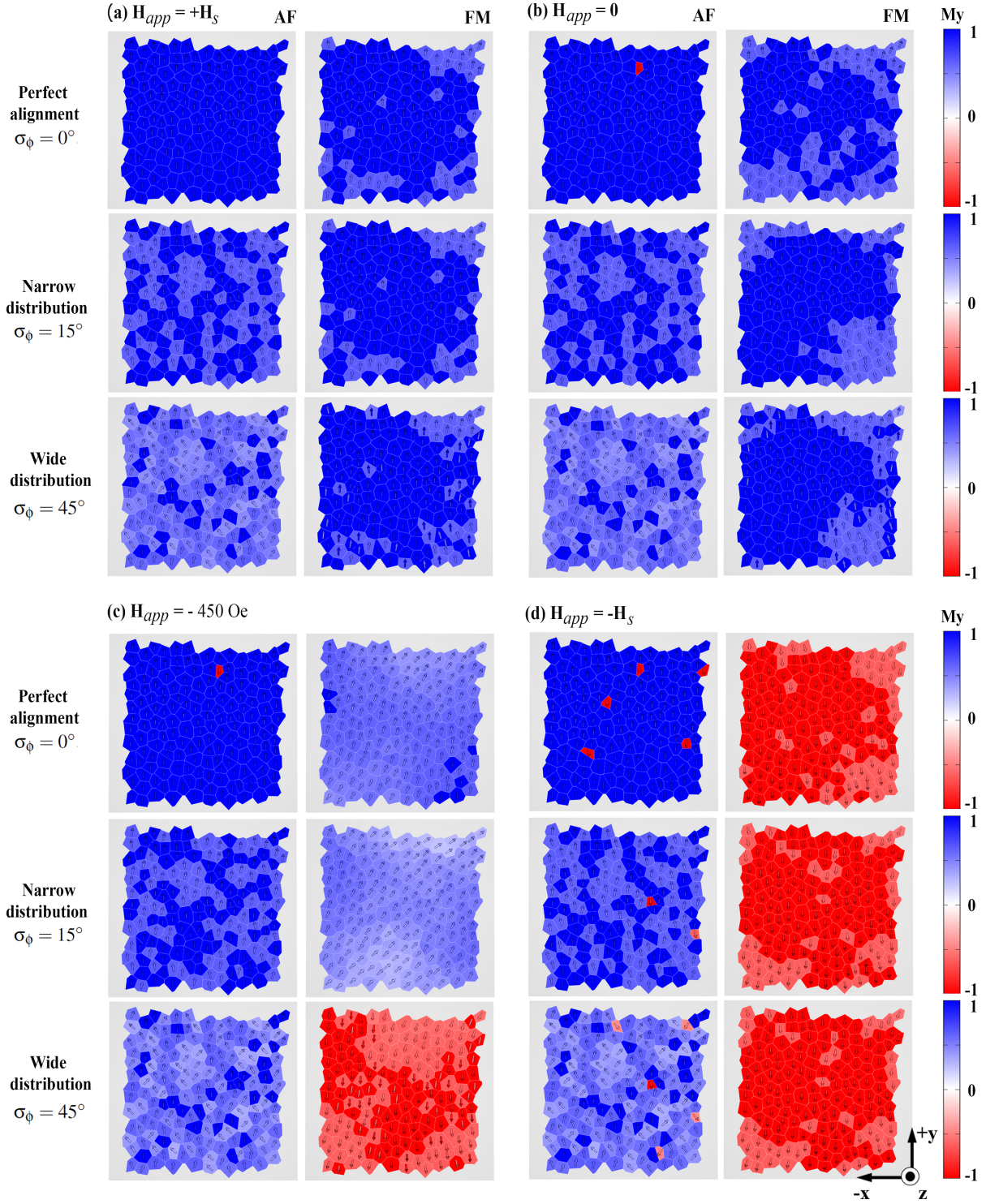
**Figure 7.** The magnetization reversal process of IrMn/CoFe exchange bias layer at different field positions in the M-H loop: positive saturation field ($+\mathbf{H}_s$), (b) zero applied field ($\mathbf{H}_{app} = 0$), (c) the applied field ($\mathbf{H}_{app}$ = -450 Oe), and negative saturation field ($-\mathbf{H}_s$). The reversal processes of the systems with perfect alignment $\sigma_\phi = 0°$, narrow distribution $\sigma_\phi = 15°$, and wide distribution $\sigma_\phi = 45°$ are also compared.

saturation field as shown in Fig.7 (a), (b), (c) and (d) respectively. Figure 7 shows visualizations of magnetization configurations for a system with lateral size of $100 \times 100$ nm$^2$. Each grain is a single domain with its individual spin direction represented by the colour scheme

shown. The top view of all grains at the interface is shown for the AF layer (left hand side) and FM layer (right hand side) for AF easy axis distributions ($\sigma_\phi = 0°$), ($\sigma_\phi = 15°$), and ($\sigma_\phi = 45°$). The magnetic parameters of CoFe and IrMn layers used in this section are $K_{FM} = 1.8 \times 10^5$ erg/cc, $K_{AF}$

= $3 \times 10^6$ erg/cc and the strength of the exchange interlayer field is $H_{ex}^{int}$ = 250 Oe.

Figure 7(a) displays the initial AF and FM microstructures. The magnetization of the FM grains is mostly aligned along the +y direction due to the applied field, while the AF orientation is dispersed in the xy plane for three cases: perfect alignment case ($\sigma_\phi = 0°$), narrow distribution case ($\sigma_\phi = 15°$) and wide distribution case ($\sigma_\phi = 45°$). Subsequently, at remanence, $\mathbf{H}_{app} = 0$, the FM magnetization is slightly rotated from the +y direction for all cases as shown in Fig. 7(b). We now proceed to reveal the magnetization reversal mechanism by considering the magnetization structures at the switching state. For the case of $\mathbf{H}_{app}$ = -450 Oe as shown in Fig.7 (c), it can be seen that the dispersion of the AF easy axes has a strong bearing on the reversal. With increasing $\sigma_\phi$ the magnetization of the AF layer becomes more non-uniform giving rise to a more non-uniform FM state. For $\sigma_\phi = 45°$ this process has led to the complete reversal of the FM layer. Interestingly, we can observe that clusters of multi-grains are not in the same orientation for wide distribution, ($\sigma_\phi = 45°$) as is clearly seen from the different red colour scheme. This feature indicates that the incoherent reversal arises from the increase of AF easy axis dispersion. We interpret this as follows. The structure of the FM layer has to respond to the random perturbations from the exchange fields from the AF layer induced by the random orientation of the AF easy axes. This induces non-uniform magnetization structures which initiate the non-coherent reversal mechanism.

Moreover, the magnetization reversal behaviour of FM grains with small AF easy axis dispersion as perfect alignment and 15° cases demonstrates the reversal of all grains almost simultaneously from blue and light blue colour respectively as shown in 7(c). The feature of reversal mechanism of narrow AF easy axis distribution shows that the magnetization orientation are parallel during reversal process. This presents the coherent reversal mode. From the visualization of it is clear that the increased angular dispersion in AF layer drives a non-coherent rotation mode in the FM layer. The impact of the wide AF easy axis dispersion also leads to the reduction of $H_{EB}$ as found in Fig.6. At $-\mathbf{H}_s$ as shown in Fig.7(d), the FM grains for each configuration are completely dominated by the strong magnetic field applied along the -y direction leading to the complete reversal. Interestingly, a few grains of the AF layers are completely switched into the -y direction by the exchange field from the FM grains.

## 4. Conclusions

A micromagnetic model of exchange bias is developed and used to investigate the magnetic properties and the reversal behaviour of CoFe grains coupled with IrMn grains. The proposed model is based on the multi-scale calculation allowing separation of two different time-scales. We included the effect of easy axis distribution and grain size distribution into the model. The variation of $H_{EB}$

as a function of magnetic parameters was investigated to provide understanding of the role of each magnetic parameter. We investigated the magnetic properties and the criterion for thermal stability of the exchange bias layer. Interestingly, the wide easy axis distribution not only strongly affects the reduction of $H_{EB}$ but also drives non-coherent behaviour in the reversal mechanism of the CoFe layer, as shown by the visualization of micromagnetic grain reversal. This confirms that the easy axis distribution is an important factor which strongly impacts the magnetic properties and exchange bias field of an exchange bias system.

## References

[1] Baibich M N, Broto J M, Fert A, Van Dau F N, Petroff F, Etienne P, Creuzet G, Friederich A and Chazelas J 1988 *Phys. Rev. lett.* **61** 2472

[2] Dieny B, Speriosu V S, Parkin S S, Gurney B A, Wilhoit D R and Mauri D 1991 *Phys. Rev. B* **43** 1297

[3] Nogués J and Schuller I K 1999 *J. Magn. Magn. Mater.* **192** 203–232

[4] Berkowitz A E and Takano K 1999 *J. Magn. Magn. Mater.* **200** 552–570

[5] Kiwi M 2001 *J. Magn. Magn. Mater.* **234** 584–595

[6] O'grady K, Fernandez-Outon L E and Vallejo-Fernandez G 2010 *J. Magn. Magn. Mater.* **322** 883–899

[7] Meiklejohn W H and Bean C P 1956 *Phys. Rev.* **102** 1413

[8] Meiklejohn W H and Bean C P 1957 *Phys. Rev.* **105** 904

[9] Vallejo-Fernandez G, Aley N P, Fernandez-Outon L E and O'Grady K 2008 *J. Appl. Phys.* **104** 033906

[10] Fulcomer E and Charap S H 1972 *J. Appl. Phys.* **43** 4184–90

[11] Vallejo-Fernandez G, Kaeswurm B, Fernandez-Outon L E and O'Grady K 2008 *IEEE Trans. Magn.* **44** 2835–38

[12] Vallejo-Fernandez G, Fernandez-Outon L E and O'Grady K 2008 *J. Phys. D: Appl. Phys.* **41** 112001

[13] De Haas O, Schäfer R, Schultz L, Barholz K U and Mattheis R 2003 *J. Magn. Magn. Mater.* **260** 380–385

[14] Zhao T, Fujiwara H, Zhang K, Hou C and Kai T 2001 *Phys. Rev. B* **65** 014431

[15] Geshev J, Pereira L G and Schmidt J E 2002 *Phys. Rev. B* **66** 134432

[16] Driemeier C, Nagamine L C C M, Schmidt J E and Geshev J 2004 *J. Magn. Magn. Mater.* **272** E811–E812

[17] Geshev J, Nicolodi S, Pereira L G, Schmidt J E, Skumryev V, Suriñach S and Baró M D 2008 *Phys. Rev. B* **77** 132407

[18] Pogossian S, Spenato D, Dekadjevi D and Youssef J B 2006 *Phys. Rev. B* **73** 174414

[19] Hu Y, Shi F, Wu G Z, Jia N, Liu Y and Du A 2013 *J. Phys. Soc. Japan* **82** 064602

[20] Dekadjevi D, Jaouen T, Spenato D, Pogossian S and Youssef J B 2011 *Eur. Phys. J. B* **80** 121–25

[21] Tarazona H, Tafur M, Quispe-Marcatoma J, Landauro C, Baggio-Saitovitch E and Schmool D 2019 *Physica B: Cond. Matt.* **567** 11–16

[22] De Siqueira J, da Silva O, Kern P, Gazola J, Carara M and Rigue J 2019 *J. Magn. Magn. Mater.* **478** 6–11

[23] Stiles M D and McMichael R D 2001 *Physical review B* **63** 064405

[24] Maitre A, Ledue D and Patte R 2012 *Journal of Magnetism and Magnetic Materials* **324** 403–409

[25] Chantrell R W, Walmsley N, Gore J and Maylin M 2000 *Phys. Rev. B* **63** 024410

[26] Callen H B and Callen E 1966 *J. Phys. Chem. Solids.* **27** 1271–85

[27] Craig B, Lamberton R, Johnston A, Nowak U, Chantrell R W and O'Grady K 2008 *J. Appl. Phys.* **103** 07C102

[28] El-Hilo M, Chantrell R W and O'Grady K 1998 *J. Appl. Phys.* **84** 5114–22

[29] Pfeiffer H 1990 *Phys. Stat. Sol. (a)* **118** 295–306

[30] Peng Y, Wu X, Pressesky J, Ju G, Scholz W and Chantrell R 2011 *J. Appl. Phys.* **109** 123907

[31] Vallejo-Fernandez G and Chapmam J N 2009 *Appl. Phys. Lett.* **94** 262508

[32] Aley N P, Kroeger R, Lafferty B, Agnew J, Lu Y and O'Grady K 2009 *IEEE Trans. Magn.* **45** 3869–72

[33] Imakita K, Tsunoda M and Takahashi M 2005 *J. Appl. Phys.* **97** 10K106

[34] Morales R, Basaran A C, Villegas J E, Navas D, Soriano N, Mora B, Redondo C, Batlle X and Schuller I K 2015 *Phys. Rev. lett.* **114** 097202

[35] Lee J, Kim S, Yoon C S, Kim C K, Park B G and Lee T D 2002 *J. Appl. Phys.* **92** 6241–6244

[36] Rodríguez-Suárez R, Vilela-Leão L, Bueno T, Mendes J, Landeros P, Rezende S and Azevedo A 2012 *Appl. Phys. Lett.* **100** 242406